ADVANCED FUNCTIONAL MATERIALS
www.afm-journal.de

Hierarchically Nanoporous Bioactive Glasses for High Efficiency Immobilization of Enzymes

Wen He, Dandan Min, Xudong Zhang, Yang Zhang, Zhiying Bi, and Yuanzheng Yue**

Bioactive glasses with hierarchical nanoporosity and structures have been heavily involved in immobilization of enzymes. Because of meticulous design and ingenious hierarchical nanostructuration of porosities from yeast cell biotemplates, hierarchically nanostructured porous bioactive glasses can provide a simple, cost-effective way to enhance catalytic activity of directly immobilized enzyme. Its unique chemical surface properties and hierarchical meso/macroporous structures lead to highly efficient catalytic performances of the directly immobilized enzymes. The enzyme molecules were spontaneously entrapped into the highly curved macropores (200–500 nm) via multipoint metal ion binding in electrical double layers. Hence, the enzyme activity and enzyme loading were enhanced, the cost of enzyme use was reduced, showing higher thermal and storage stabilities than free enzyme. The reactant and products of catalytic reactions can freely diffuse through open mesopores (2–40 nm). The formation mechanism of hierarchically structured porous bioactive glasses, the immobilization mechanism of enzyme and the catalysis mechanism of immobilized enzyme are then discussed. The novel nanostructure with advanced properties is expected to be utilized as a solid support for any enzyme for bioconversion, bioremediation, biosensors and drugs.

1. Introduction

Improvements of biocatalytic efficiency and enzyme stability for preparing biochemical products, biosensors and drugs can be achieved by manipulating the structure of carrier materials.[1,2] Mesoporous (2–50 nm) inorganic materials can sustain high enzyme loading, reduce the required amount of enzymes, prolong the lifetime of enzyme reactors and increase the potential for enzyme reuse, but suffer a serious diffusional problem for the catalytic reactions of enzymes. Particularly the poor biocompatibility of these materials is a big hurdle for directly immobilizing enzymes. The surface of these materials needs intricate modification.[3] Recently, the sol-gel derived mesoporous silica has begun to attract attention for enzyme immobilization and drug delivery.[4–6] The enzyme confinements in the nanochannels generate synergistic effects that enhance enzyme stability, facilitate separation and reuse of enzymes. However, owing to the small pore size and non-open-pore structure of the mesoporous inorganic materials, the enzymes in these materials exhibit lower specific activity than the free enzymes in solution.[7] Mesoporous bioactive glasses obtained by sol-gel process have attracted much attention because of their high bioactivity, biocompatibility, porosity, chemical homogeneity and applications in tissue repair and replacement and drug carriers.[8,9] However, the great potential of bioactive glasses for enzyme entrapment has not yet been realized.

Glucose oxidase (GOD), amylase and catalase are the protein catalysts with high efficiency and specificity for food industry,[10] medicine and clinical applications.[11] Recently, some researchers have studied immobilization of various enzymes on different solid supports in order to enhance its catalytic activity, reusability, operational stability, and ability to withstand extreme conditions.[12–14] Divalent metal ions (such as Zn^{2+}, Ca^{2+} and Mg^{2+}) play a critical role in catalysis by many RNA and protein enzymes. They can serve as electron donors or acceptors, Lewis acids or structural regulators that participate directly in the catalytic process.[15] Immobilization of glucose oxidase onto zinc oxide has been investigated by many researchers in the field of biosensors since it is a promising support material for enzymes.[16,17] Incorporation of modifiers such as zinc, magnesium, cerium and gallium into a series of bioactive glass has also been conducted to improve specific performances for tissue repair and replacement and drug carriers.[18,19] However, to the best of our knowledge, the ZnO-containing bioactive glass has not been used as enzyme supporting material.

In nanotechnology applications, great attention has been paid to biomaterial systems to discover new self-assembly techniques. The interaction of nanoparticles with proteins, peptides, and DNA has been studied for innovative and robust nanomaterial designs.[20,21] Nanobiotechnology is one of the most powerful routes for organizing a nanoscale system with

Prof. W. He, D. D. Min, Prof. X. D. Zhang, Z. Y. Bi, Prof. Y. Z. Yue
Shandong Key Laboratory of Glass and Functional Ceramics
Qilu University of Technology
Jinan, 250353, PR China
E-mail: zxd1080@126.com; yy@bio.aau.dk
Prof. Y. Z. Yue
Section of Chemistry
Aalborg University
DK-9000 Aalborg, Denmark
Dr. Y. Zhang
College of Engineering
Ocean University of China
Qingdao, 266100, China

DOI: 10.1002/adfm.201303278

the highest possible accuracy and control. Biological systems can produce extraordinary inorganic structures and morphologies.[22–25] Integrating bioactive carrier materials with enzyme is a simple, cost-effective way to enhance catalytic activity of directly immobilized enzyme. In this work we synthesize a bioactive glass with hierarchical nanostructures in the system ZnO-CaO-SiO_2-P_2O_5 (ZCSP-BNG) via the sol-gel approach and using yeast cells as biotemplates. We introduce a conceptually new approach of directly immobilizing enzyme, in which Zn^{2+} and Ca^{2+} ions in an electrical double layer on the macroporous wall of ZCSP-BNG provide high affinity for enzyme molecules and have a beneficial effect on enzyme's immobilization and catalytic performance. This work provides insights into the formation mechanism of ZCSP-BNG, the immobilization mechanism of enzyme and the catalysis mechanism of immobilized enzyme. By using the unique immobilization approach, we attempt to reach the following goals: (1) In comparison with those reported in literatures (Supporting Information Table S1), high biocompatibility of ZCSP-BNG with enhancing enzyme activity; (2) High enzyme loading (>95%), high thermal and storage stabilities due to the sufficiently large pore size (200–500 nm) and high negative surface curvature without leakage problem of entrapped enzyme; (3) High biocatalytic efficiency because of enhancing diffusion rates of reactants and products via mesopores (2–40 nm) and lamellar structure.

2. Results and Discussion

2.1. Formation Mechanism of ZCSP-BNG

In our approach (**Figure 1**), to ensure the formation of colorless and transparent sols, citric acid was added to promote and stabilize the hydrolysis of tetraethyl orthosilicate (TEOS) and triethyl phosphate (TEP).[26] When the precursor solutions were mixed in certain ratio, water molecular directly attacks TEOS and TEP in an acid medium (pH = 1), and induces the hydrolysis reaction. The hydrolysis of TEOS and TEP slows down and $M(OR)_3OH$ (M is Si or P) dominates when the dosage of distilled water is not enough for the further hydrolysis of TEOS or

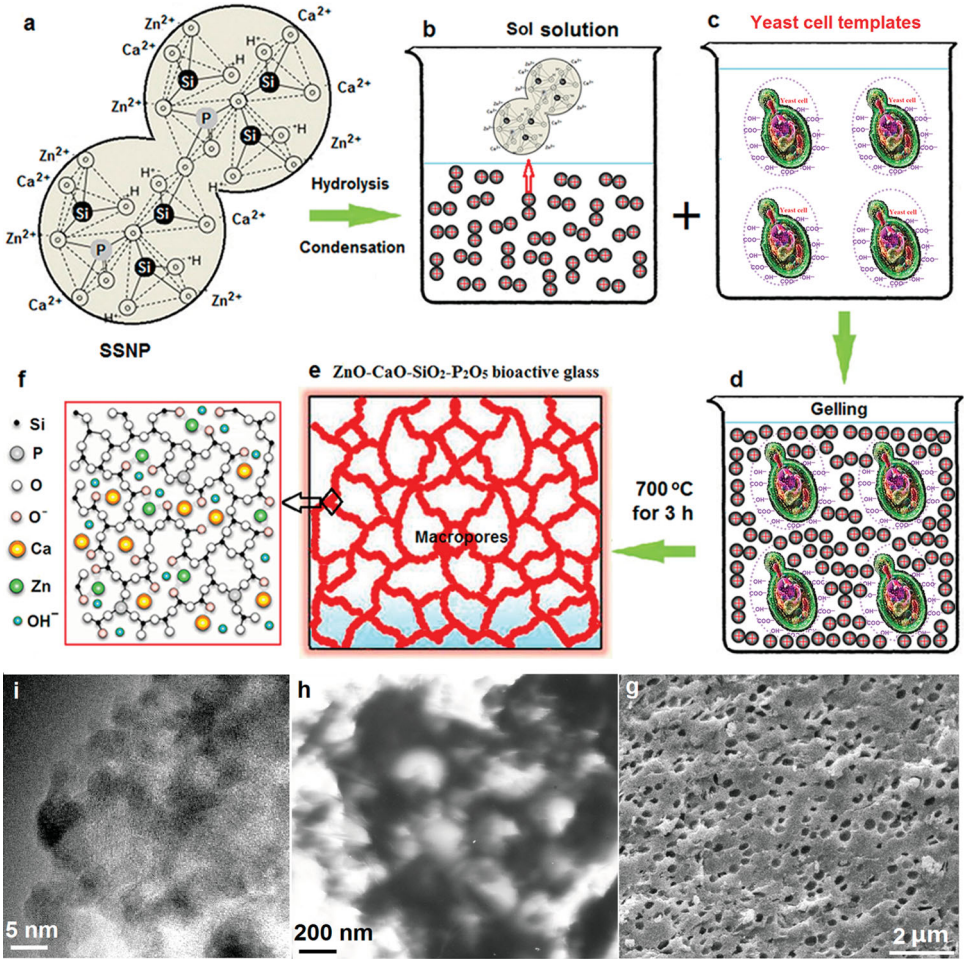

Figure 1. Schematic of synthesis of ZCSP-BNG. a) Hydrolysis and condensation of TEOS and TEP, and formation of a linear phosphor-silcate polymer structure. b) Formation of positively charged sol solid nanoparticles and a colorless and transparent sol phase. c) Yeast cell biotemplates. d) Aggregation of sol nanoparticles on the surface of yeast cell particles and formation of three dimensional gel network structure. e) Macropores in the scaffolds of ZCSP-BNG. f) Nanovoids between different network fragments in ZCSP-BNG. (g) SEM image of 10ZCSP-BNG(15) sample. (h) TEM image of 10ZCSP-BNG(15) sample. (i) HRTEM image of 10ZCSP-BNG(15) sample.

TEP. Water produced from the dehydration condensation of silicon and phosphorus alkoxide mixture can partially promote the hydrolysis of TEOS and TEP.[27] Therefore, the dealcoholization condensation dominates over the dehydration condensation. Hydrolysis promotes the formation of Si–O–Si, Si–O–P, and P–O–P linear chains, which in turn interact with each other, and form a linear phosphor-silcate polymer structure (Figure 1a).[28] The condensation further leads to the formation of positively charged sol solid nanoparticles (SSNPs) with a diameter of few hundreds of nm suspended in a colorless and transparent sol phase (Figure 1b). The yeast cell templates was employed in the sol-gel process to induce the formation of the macropores in ZCSP-BNG. The proteins and polysaccharides in yeast cell have hydrophilic anion groups and negative charges (Figure 1c).[29] Like most natural cells, yeast cells can induce spontaneous mineralization on its surface, due to the relatively low charge density.[30] When the sol solution is added to the yeast cell solution, the positively charged SSNPs can self-assemble on the surface of yeast cells via electrostatic adsorption (Figure 1d). In the process of gelling, as the SSNPs condense, a three dimensional gel network structure froms. The yeast cells act as organic templates to avoid the collapse of the porous gel network structure during the drying course (60 °C). After heat treatment at 700 °C for 3 h, the yeast cells and citric acid molecules were removed, leading to the formation of both macropores in the scaffolds of ZCSP-BNG (Figure 1e) and nanovoids between different network fragments in ZCSP-BNG (Figure 1f). The pore size of the ZCSP-BNG is a vital parameter in the enzyme immobilization. To understand the effect of yeast cell biotemplates on the porous structure of synthesis materials, we characterized the structure of synthesized samples using scanning electron microscope (SEM) and high-resolution transmission electron microscopy (HRTEM). SEM and TEM images show that the 10ZCSP-BNG(15) sample owns the sufficiently large pore size (200–500 nm) (Figure 1g and 1h) and negative surface curvature (Supporting Information Table S2).[31] These macropores provide high enzyme loading without leakage problem of entrapped enzyme. The HRTEM image of 10ZCSP-BNG(15) sample shows amorphous phase without lattice fringes and open connected mesoporous domains (high brightness regions, 2–40 nm) (Figure 1i). Through SEM and HRTEM results, we have verified that the formation mechanism in Figure 1 is feasible for synthetizing ZCSP-BNG. This hierarchical pore structure may facilitate the process of different enzyme immobilization and catalyt reactions and have a wide range of applications.

2.2. Characterizations of ZCSP-BNG

To understand the effect of zinc oxide content on glass structure, we characterized the ZCSP-BNGs using various methods as shown in **Figure 2**. In Figure 2a, the XRD curve of each

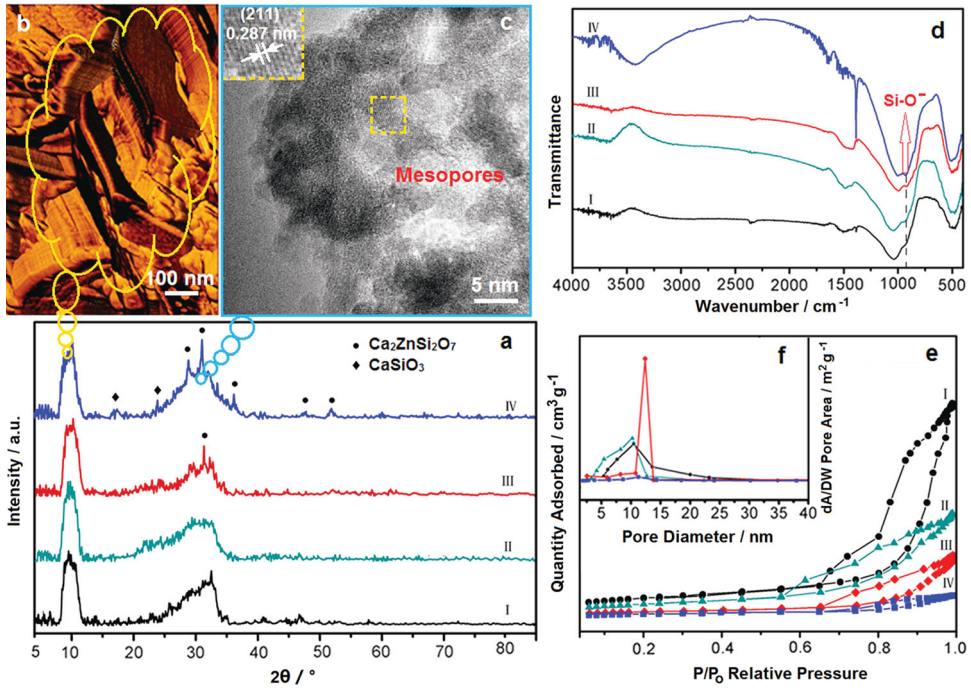

Figure 2. Structure characterizations of ZCSP-BNGs synthesized with different zinc oxide content. All samples synthesized with 10% Yeast/TEOS weight ratio, and the samples synthesized with different zinc oxide contents (0, 5, 10 and 15 mol%) were denominated as 10ZCSP-BNG(0), 10ZCSP-BNG(5), 10ZCSP-BNG(10) and 10ZCSP-BNG(15), respectively. a) XRD patterns of ZCSP-BNG samples synthesized with different zinc oxide contents. Hardystonite ($Ca_2ZnSi_2O_7$, PDF file 35–745) (●) and Wollastonite ($CaSiO_3$, PDF file 42–547) (◆) peaks are demarcated. b) The atomic force microscopy (AFM) image of layer structure in 10ZCSP-BNG(15). Scale bar, 100 nm. c) HRTEM image of mesoporous network structure and nanocrystals in 10ZCSP-BNG(15). Scale bar, 5 nm. d) FTIR spectra of ZCSP-BNG samples synthesized with different zinc oxide content. ef) N_2 adsorption-desorption and pore size distribution curves (inset) of ZCSP-BNGs synthesized with different zinc oxide contents. I) 10ZCSP-BNG(0),II) 10ZCSP-BNG(5), III) 10ZCSP-BNG(10), IV) 10ZCSP-BNG(15).

sample shows two broad main peaks, because of the amorphous phase and the layered structures in the composite, and both peak width and intensity increase with zinc oxide content. In the 2θ range of 8 to 12°, each XRD curve shows a strongest and broad diffraction peak, which is assigned the layered structures with different interlamellar spacings (0.55–0.37 nm) in ZCSP-BNG. The atomic force microscopy (AFM) image of 10ZCSP-BNG(15) further confirms its layer structure (Figure 2b). In the 2θ range of 25 to 34°, each curve shows a broad bump, indicating amorphous nature of the samples. However, some weak peaks appear on the broad bump when ZnO reaches 10 mol.%, and they become even sharper when ZnO reaches 15 mol.%, indicating that the degree of local structural ordering can be enhanced by increasing the ZnO content. The local ordering and thus induced nucleation causes the contraction of local volume and hence the voids form, which can grow into nanopores with increasing the heat-treatment degree (temperature or time).[32,33] This process is particularly intense when more ZnO is introduced. At 15 mol.% ZnO, the hardystonite and wollastonite nanocrystals form (Figure 2aIV), indicating that the glass forming ability of the 15 mol.% ZnO, containing glass is relatively low. This can be attributed to the low network connectivity of this glass, i.e., to the relatively high average number (1.72) of non-bridging oxygen per Si-tetrahedron.[34] The HRTEM image of 10ZCSP-BNG(15) shows nanocrystalline phase (Figure 2c inset) and open mesoporous domains (Figure 2c). In addition, we studied the effect of zinc oxide content on the network connectivity of ZCSP-BNG by FT-IR spectra (Figure 2d). The FTIR spectra show that the intensity of the absorption band at 912 cm^{-1} for Si-O (non-bridging oxygen) stretching vibration increases with zinc oxide content (Supporting Information Table S3), but its peak position does not change, and a new band at 1385 cm^{-1} for Zn-O bond is seen. This means that the zinc ions breaks glass network, and hence, the slit like nanopores are easily generated. The adsorption-desorption isotherms (Figure 2e) and BJH pore-size distribution curves (Figure 2e inset) of the synthesized samples show that the H3 isotherm caused by uneven slit shape pores is transformed into the H4 isotherm caused by uniform slit shape pores[35] and the surface area increases with the amount of ZnO (Supporting Information Table S3). This result is consistent with the XRD and FTIR results described above.

To determine the biocompatibility of different ZCSP-BNG samples, L-929 fibroblasts were exposed to the leaching solution of different ZCSP-BNG samples. The relative proliferation rate values of L-929 fibroblasts assessed using MTT-based methods at different time points of incubation are shown in **Figure 3**a. It can be seen that the relative proliferation rate values for all samples are greater than 75%, which indicates that all ZCSP-BNG samples have no negative effect on the viability proliferation of L-929 fibroblasts, and that they have good biocompatibility.[36,37] The concentration of zinc ions released from 10ZCSP-BNG(15) particles and 10ZCSP-BNG(15)-GOD in HAc-NaAc buffer solution as related to the time are shown in Figure 3b, showing some degradation of ZCSP-BNG. The standard curve for zinc ion solution at ambient temperature see Supporting Information Figure S1. High biocompatibility and biodegradablity of ZCSP-BNG can enhance the enzyme activity.

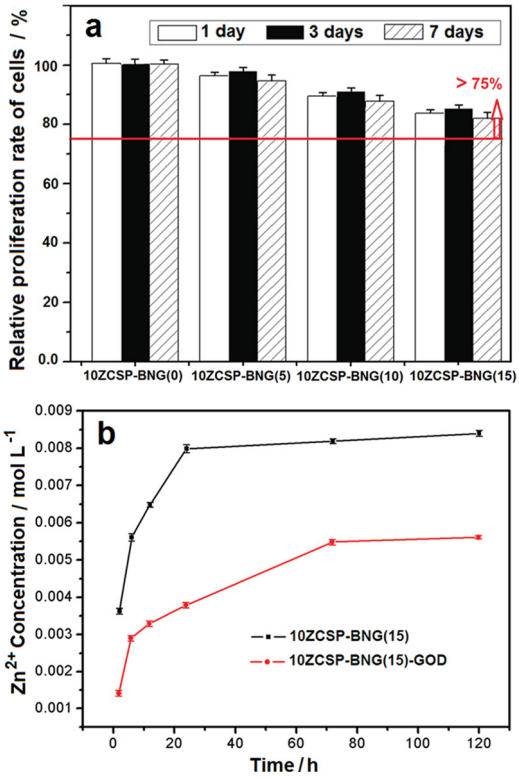

Figure 3. Biocompatibility and tests in vitro. a) The relative proliferation rates of L-929 fibroblasts assessed using MTT-based methods at different time points of incubation and in the leaching solution of different substrates (P>0.05). The data are presented as means ±standard errors of the means (n = 3). b) The concentration of zinc ions released from 10ZCSP-BNG(15) particles and 10ZCSP-BNG(15)-GOD in HAc-NaAc buffer solution as related to the time. n = 5; data are means±s.d.

2.3. Properties and Characterizations of Immobilized Enzymes

We investigated the properties of Glucose oxidase (GOD),amylase and catalase immobilized on different bioactive glass supports. The influence of ZCSP supports synthesized with different Yeast/TEOS weight ratio on GOD activity and amount of GOD loading is summarized in **Figure 4**a. It is observed that GOD immobilized onto 10ZCSP-BNG(15) has a highest activity at 401 Ug^{-1} (2.28 times that of 0ZCSP(0)), a maximum load (95.2%) and an exceptionally high immobilization efficiency of near 100% (i.e., the ratio of the specific activity of the immobilized GOD to that of the free GOD in solution is almost 1) because the 10ZCSP-BNG(15) sample has the higher surface area of 198.56 $m^2 g^{-1}$ (see Supporting Information Table S2 and Table S3). At least 82% of its initial activity of 10ZCSP-BNG(15)-GOD was still reserved after 14 times of reuse (Figure 4c), it reduces the cost of enzyme use (per kg ZCSP-BNG can save 10–23 g GOD). In addition, 10ZCSP-BNG(15)-GOD exhibits excellent operation adaptability in the temperature range 50–80 °C than free GOD (Figure 4d). Figure 4b shows that the activity of GOD immobilized on the 0ZCSP, 10ZCSP-BNG and 10FCSP samples increases with increasing the ZnO and Fe_2O_3 content, which indicates that Zn^{2+} and Fe^{3+} ions play a critical role in the activation of GOD

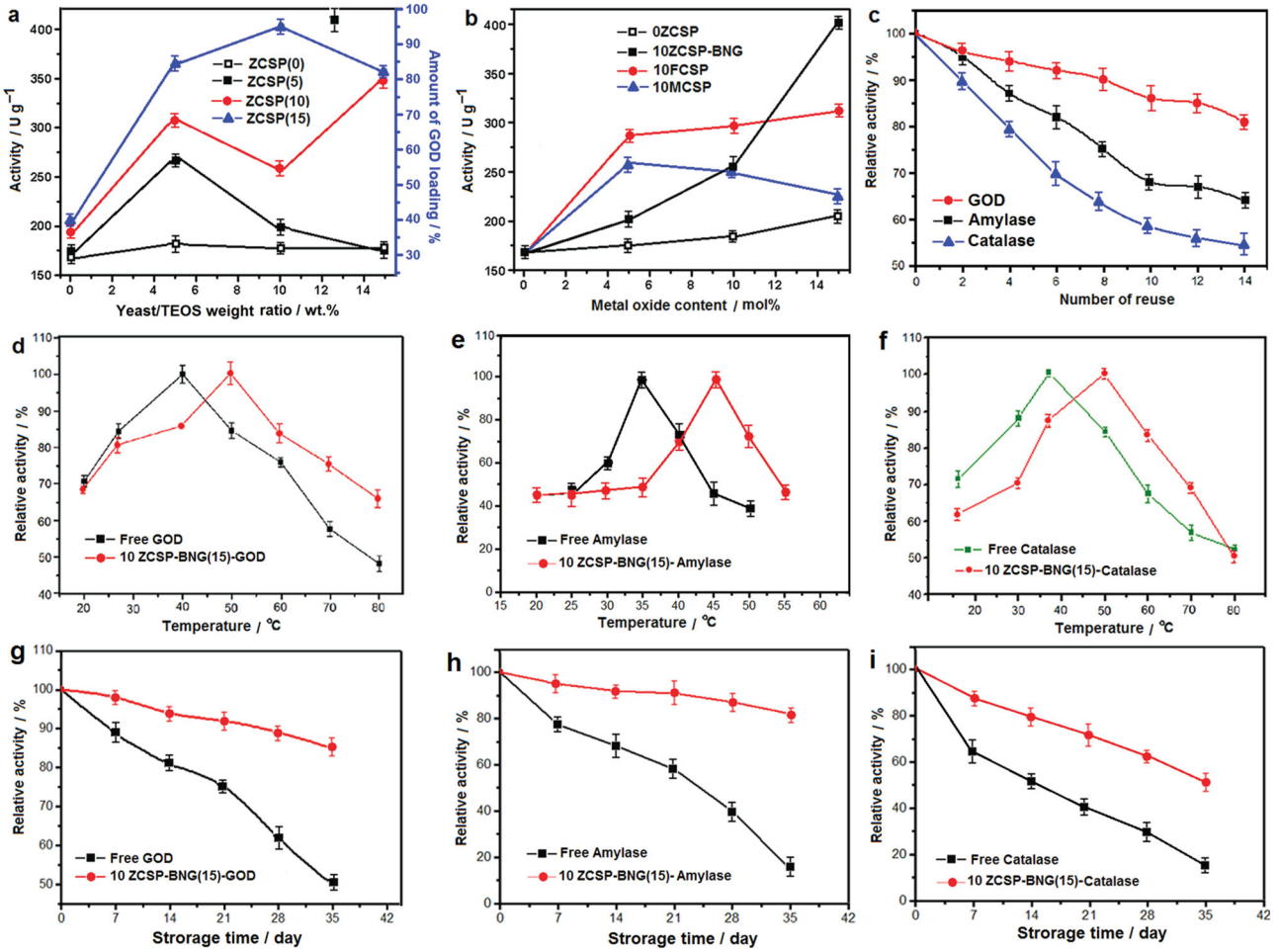

Figure 4. Properties of various enzymes directly immobilized on different supports. a) GOD activity and amount of GOD loading in ZCSPs synthesized with differentYeast/TEOS weight ratio. b) Activity comparison of supports synthesized with different metal oxide content for GOD immobilization. c) Relative activity of different enzymes immobilized on10ZCSP-BNG(15) as a function of reuse numbers. d) Thermal stability of free GOD and immobilized 10ZCSP-BNG(15)-GOD at different reaction temperature, pH 6 for 12 h. e) Thermal stability of free amylase and immobilized 10ZCSP-BNG(15)-Amylase at different reaction temperature, pH 7 for 12 h. f) Thermal stability of free catalase and immobilized 10ZCSP-BNG(15)-Catalase at different reaction temperature, pH 6 for 12 h. g–i) Storage stability of free enzymes and various enzymes directly immobilized on 10ZCSP-BNG(15) at at 4 °C. n = 5, data are means±s.d.

catalysis. When the MgO content is more than 5%, the activity of GOD immobilized on the10MCSP samples decrease with increasing it, this shows that Mg^{2+} ions inhibit the enzymic activities. This also means that 10ZCSP-BNG(15) is an ideal material for both high loading amount and immobilization efficiency. In Figure 4c, the remaining activity of immobilized amylase and catalase were about 64% and 54% after 14 cycles of batch operations, respectively. Temperature profiles of free and immobilized amylase and catalase are shown in Figure 4e and f, respectively. The activity loss of immobilized amylase and catalase also was less than the free enzyme for higher temperature. 10ZCSP-BNG(15) support might have a protecting effect at the high temperatures at which enzyme deactivation takes place. In addition, Free and immobilized enzymes were stored in a phosphate buffer (40 mM, pH 6.0) at 4 °C and the activity measurements were carried out for a period of 35 days. The free GOD lost 50% of its activity and immobilized GOD lost 25% of its activity within 35 days (Figure 4g). Both amylase and catalase immobilized on the10ZCSP-BNG(15) also showed higher storage stabilities than free enzymes (Figure 4h and i). The immobilization process provided an advantage in the stability of enzyme over free enzyme activity, especially at longer durations.

We characterized the immobilization of GOD onto ZCSP-BNG using various methods as shown in **Figure 5**. Atomic force microscopy (AFM) images clearly show that the surface morphology (Figure 5a) of 10ZCSP-BNG(15) with layered nanostructure appears to be completely covered by a thick and strongly attached GOD molecular layer (Figure 5b), where aggregates of GOD, as compared to the molecular dimensions, can be seen. The charge density of metal ions would reduce the electrostatic repulsion of GOD molecules, leading to GOD aggregation and large surface coverage onto the surface of ZCSP-BNG.[38] This result shows that the aggregates of GOD molecules are evenly distributed onto the surface of ZCSP-BNG. N_2 adsorption and desorption isotherms and the

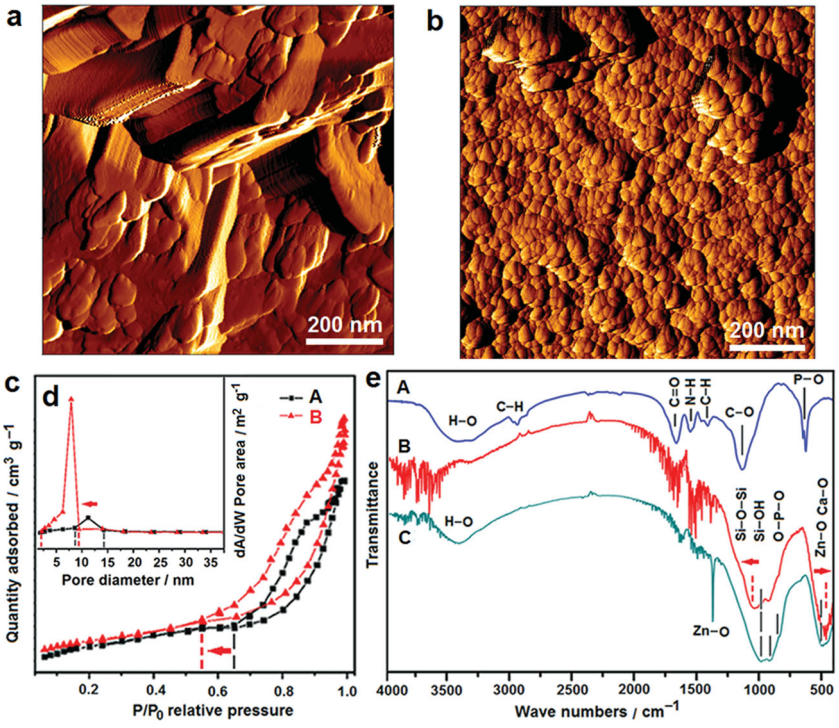

Figure 5. Characterizations of GOD immobilized on 10ZCSP-BNG(15). a,b) The surface appearance comparison of 10ZCSP-BNG(15) samples before (a) and after (b) GOD immobilization treatment by AFM images. Scale bar, 200 nm. cd) The mesoporous structure comparison of 10ZCSP-BNG(15) samples before and after GOD immobilization by (c) N_2 adsorption-desorption and (d) pore size distribution curves. e) FTIR spectra analysis: (A) FTIR spectrum of pure GOD; (B) FTIR spectrum of 10ZCSP-BNG(15)-GOD; (C) FTIR spectrum of 10ZCSP-BNG(15).

pore size distribution curves were used to analyze the pore parameter change of 10ZCSP-BNG(15) and 10ZCSP-BNG(15)-GOD. The type and profile of its adsorption isotherm show no changes after GOD immobilization, but the isotherm of 10ZCSP-BNG(15)-GOD has shifted to a lower relative pressure (Figure 5c) and show the slight upward profile. Especially the pore size distribution after GOD immobilization has narrowed down to 2–9 nm from 8–14 nm before GOD immobilization and the adsorbed volume of nitrogen increases (Figure 5d). This indicates that the GOD molecules with an average diameter of 8 nm can be immobilized inside the mesopores in the range of 8–14 nm due to their strong adsorption ability to N_2. These results further verify that GOD has been immobilized on 10ZCSP-BNG(15). The chemical bond linkages between GOD molecules with the metal ions on the surface of ZCSP-BNG were studied by Fourier Transformation Infrared (FT-IR) spectra. By comparing, the following four changes are seen from FTIR spectra in Figure 5e. First, in the FTIR spectrum of 10ZCSP-BNG (15)-GOD (Figure 5eB), the absorption band in 3,250 to 3,635 cm^{-1} has shifted to a higher wavenumber from pure GOD (Figure 5eA) and 10ZCSP-BNG (15) (Figure 5eC) and produced fission. Second, the Ca-O and Zn-O vibration peaks in 250 to 600 cm^{-1} for the 10ZCSP-BNG(15) have shifted to a lower wavenumber and become sharp, broad. Thirdly, the Si-O-Si asymmetric stretching vibration was shifted to a higher wave number. Finally, the absorption bands at 1385 cm^{-1} for Zn-O and C-O bond of residual carbon in 10ZCSP-BNG(15) and 1,695 cm^{-1} for Amide IV and/or Amide V in pure GOD disappeared. This means that the interactions between the Zn^{2+} and Ca^{2+} ions on the surface of ZCSP-BNG and the negatively charged -COO^-, OH^- and -OPO_3^{2-} groups in the amides of GOD molecules are chemical bonds in nature, which can be identified by the wave number shift, vibration intensity change and disappearance on some absorption bands in the ZCSP-BNG-GOD spectrum. These chemical bonds play an important role in high biocatalytic efficiency and long lifetimes of immobilized enzymes.

2.4. Immobilization and Catalysis Mechanisms of GOD onto ZCSP-BNG

GOD is a dimeric anionic protein with the 3D structure and is covered with negatively charged carbohydrate chains and P-O bonds. The oxidation reaction is performed by the active sites of flavin adenine dinucleotide (FAD) cofactors bound deeply inside GOD. FAD can exist in two redox states that can be converted to each other by accepting or donating electrons. The primary structure of the GOD molecule is a slightly elongated globular protein with an average diameter of 8 nm and a partial specific volume of 0.75 ml g^{-1}, which is high soluble in water.[39] Zn^{2+} and Ca^{2+} are easily electrostatically bond to negatively charged species. As a Lewis acid and a redox centre they can balance the negative charges of the enzyme and hence activate substrates. The enzymic catalytic reaction is accomplished primarily by coordination of the enzymic molecule to a metal ion that is bound in the active site of the enzyme. Nanostructure and surface chemical features of ZCSP-BNG could exert effect on immobilization of GOD and its catalytic properties.[40,41] Immobilization mechanism of GOD on ZCSP-BNG is described in **Figure 6**. When GOD was incubated with the ZCSP-BNG in the phosphate buffer solution, the GOD molecules were spontaneously entrapped into the macroporous structure of ZCSP-BNG, and this is proven by the TEM image (Figure 6a) of 10ZCSP-BNG(15) after immobilization. In the macroporous structure of ZCSP-BNG, the GOD molecules were bound to the porous wall and stabilized by the Zn^{2+} and Ca^{2+} ions via electrostatic interaction, resulting in a metal-activated enzyme, as shown in Figure 6b. In the meantime, microenvironment in macropore determines the accessibility of active sites and the configuration of the enzymes. Zn and Ca cofactors become an important part of the active sites of GOD molecules, and promote the conformational change of enzyme molecules. GOD molecules loosen the structure at its active site, and exposes redox catalytic centres to an "open conformation", allowing substrates to easily access to the active site.[42,43] The catalytic active sites are represented as red hexagonal stars (Figure 6b). The open nanoporous structure in ZCSP-BNG promotes an increase of diffusion rates of reactants from the

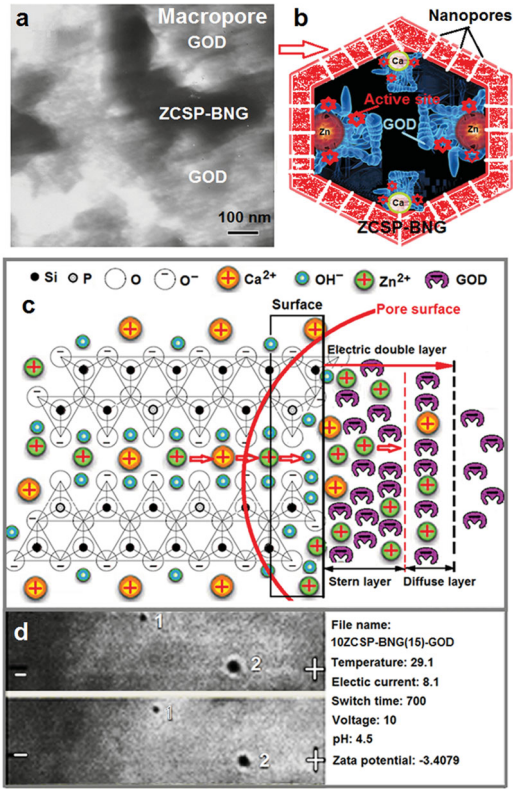

Figure 6. Immobilization mechanism of GOD on 10ZCSP-BNG (15). a) TEM image of 10ZCSP-BNG (15) after immobilization. Scale bar, 100 nm. In b), Zn and Ca cofactors exposed redox centres, catalytic active sites are represented as red hexagonal stars. c) Schematic of the electric double layer immobilization of GOD inside the macroporous of ZCSP-BNG. d) Micro electrophoresis images of the 10ZCSP-BNG(15) sample after immobilization, symbolized by 10ZCSP-BNG(15)-GOD.

solution towards the active site. On the other hand, during the catalytic reaction stage, the complex needs to have an open coordination site for the substrate.[44]

A previous study shows that an electric double layer (EDL) can form on the surface of macropores of ZCSP-BNG in buffer solution and its surface curvature is an important factor promoting the immobilization of GOD.[45] In Figure 6c, the interface of electric double layer (EDL) can be divided into an inner region (Stern layer) and an outer region (diffuse layer). In the inner layer, Ca^{2+} and Zn^{2+} are immobilized because they are either strongly attracted to the surface by electrostatic interactions, or specifically adsorbed onto the charged surface due to van der Waals force, hydrogen bonding, or other binding mechanisms. The diffuse layer is composed of mobile ions and their distribution depends on the electrostatic interaction and on thermal diffusion.[46]

The formation mechanism expression of surface electric double layer inside the macropore of ZCSP-BNG is as follows:

1) There are many ≡Si–O–Ca–O–Si≡, ≡P–O–Ca–O–P≡ and ≡P–O–Zn–O–P≡ ionic groups in the network structure of ZCSP-BNG, symbolized by $(\equiv Si–O)_2Ca$, $(\equiv P–O)_2Ca$ and $(\equiv P–O)_2Zn$, respectively. Ca^{2+} and Zn^{2+} combine with two non-bridged oxygens via ionic bonding. Both Ca^{2+} and Zn^{2+} on the surface (symbolized by g) exchange with H^+ in the solution and diffuse into the solution (symbolized by s). The silica and phosphorus groups form and this makes surface negatively charged.

$$(\equiv Si–O)_2\,Ca(g) + 2\,H^+\,OH^- \rightarrow 2(\equiv Si–OH)(g) + 2\,OH^-(s) + Ca^{2+}(s) \quad (1)$$

$$(\equiv P–O)_2\,Ca(g) + 2\,H^+\,OH^- \rightarrow 2(\equiv P–OH)(g) + 2\,OH^-(s) + Ca^{2+}(s) \quad (2)$$

$$(\equiv P–O)_2\,Zn(g) + 2\,H^+\,OH^- \rightarrow 2(\equiv P–OH)(g) + 2\,OH^-(s) + Zn^{2+}(s) \quad (3)$$

Cations in the solution enter into the inner layer of the electrical double layer and make the inner layer positively charged. The inner layer positively charged can adsorb and immobilize the GOD molecules negatively charged in the solution to form the electrical double layer.

2) The ion chemical potential in the electrical double layer can be expressed as:[47]

$$\mu_{iD} = \mu^o_{iD} + RT\ln\alpha_{iD} + Z_i F\phi_o \quad (4)$$

And the ion chemical potential in the bulk solution is given by:

$$\mu_{iB} = \mu^o_{iB} + RT\ln\alpha_{iB} \quad (5)$$

where μ^o_{iD} and μ^o_{iB} are the standard chemical potentials of ions in the electrical double layer and the bulk solution, respectively. α_{iD} and α_{iB} are the ionic activities in the electrical double layer and the bulk solution, respectively. Zi is the ion valence, Φ_0 is the surface potential of the material and F is the Faraday's constant (C mol^{-1}).

In standard state

$$\mu^o_{iD} = \mu^o_{iB} \quad (6)$$

When the electrical double layer and the bulk solution are in equilibrium, we have then:

$$\mu_{iD} = \mu_{iB} \quad (7)$$

$$\text{or}: \mu^o_{iD} + RT\ln\alpha_{iD} + Z_i F\phi_o = \mu^o_{iB} + RT\ln\alpha_{iB} \quad (8)$$

We get from Equations (7) and (8):

$$\alpha_{iD}/\alpha_{iB} = \exp(-Z_i F\phi_O/RT) \quad (9)$$

Beacause the surface potential (Φ_0) of ZCSP-BNG is a negative value it makes $\exp(-Z_i\,F\Phi_0/RT)$ always greater than 1, so $\alpha_{iD} > \alpha_{iB}$, indicating that the ionic activity in the electrical double layer is higher than that of the bulk solution.

OH^-anions can balance one part of positive charges on the surface and between the interlaminated layers. The negative curvature of the macroporous surface can improve the stability of OH^-on the surface, increase the active sites of metal ions and enhance the GOD loading. In the inner layer, the Zn^{2+} and Ca^{2+} concentration is higher than that of the bulk solution due to the degradation of ZCSP-BNG (Figure 3b), strong adsorption and higher ionic activity. This is why both the immobilized sites and the bond strength of the GOD increase, and chemical driving force increases significantly. As stated above, the EDL theory could explain the high activity and storage stability of immobilized GOD inside the macropores of ZCSP-BNG. Evidence for EDL formation was obtained using

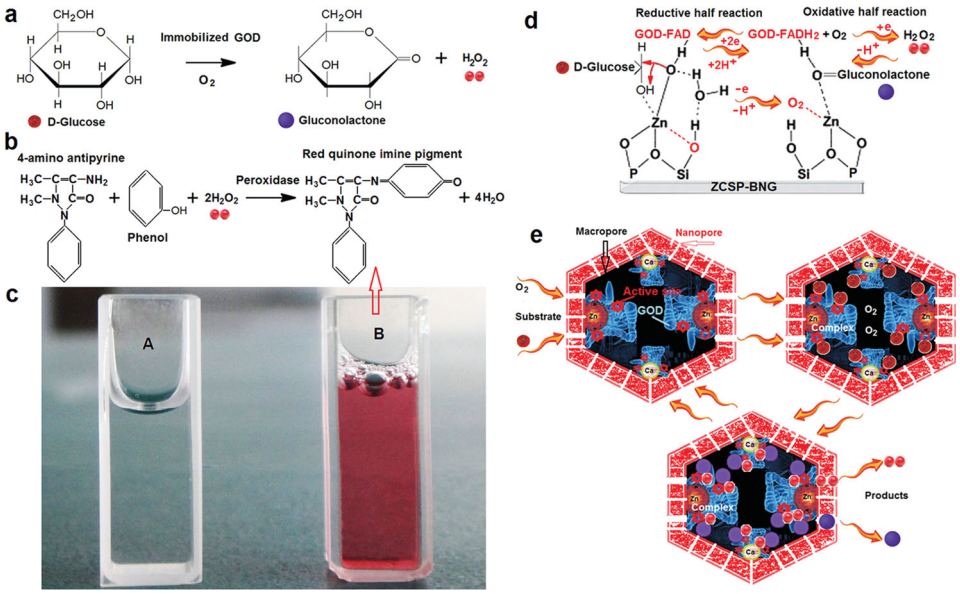

Figure 7. Catalytic mechanism of immobilized GOD. a) Catalytic reaction equation of GOD immobilized onto ZCSP-BNG. Immobilized GOD catalyzes the oxidation of glucose (brown-red sphere) to produce gluconolactone (purple sphere) and hydrogen peroxide (red sphere) in the presence of oxygen. b) Formation equation of red quinoneimine dye in the immobilized GOD enzyme assay. c) Images of the immobilized GOD enzyme assay. d) Schematic of the redox reaction of GOD immobilized onto ZCSP-BNG and a simple overview of electron transfer among immobilized GOD, substrate and products. e) Schematic of the modulating catalytic reaction of immobilized GOD. The substrate-enzyme and product-enzyme complexes are depicted. The colour coding is similar to that of the corresponding schematic displays.

JS94H micro-electrophoresis (Figure 6d). The zeta potential of 10ZCSP-BNG(15)-GOD particle is −3.41, indicating that there are superfluous negative charges on the particle surface. Thus, we infer that the multipoint metal ion binding immobilization mechanism of GOD in the EDL is feasible.

Catalytic mechanism of immobilized GOD is described in **Figure 7**. In a GOD-catalyzed reaction, the immobilized GOD catalyzes the oxidation of glucose substrate (symbolized by brown-red sphere) to produce gluconolactone (symbolized by purple sphere) and hydrogen peroxide (symbolized by red sphere) products in the presence of oxygen (Figure 7a). Activity of free and immobilized GOD can be determined by measuring the initial rate of formation of hydrogen peroxide at a given temperature following the formation of a red quinoneimine dye, as mentioned by Rauf et al.[48] Once phenol and 4-AAP encounter peroxidise (POX) in the mixed solution react with hydrogen peroxide, a red quinoneimine dye is produced and determined at 500 nm using a 7200 Visible Spectrometer (Figure 7b,c). The absorbance of quinoneimine dye is proportional to the concentration of glucose in the sample. The protonation of various amino acids in enzyme molecules is an important factor influencing the stability of enzyme structures.[7] FAD (fully oxidized form, or quinone form) in GOD structure accepts two electrons and two protons to become $FADH_2$ (hydroquinone form). $FADH_2$ is an energy-carrying molecule, because, if it is oxidized, it will release all the energy of this stabilization. The primary biochemical role of $FADH_2$ in the redox reaction of GOD is to carry high-energy electrons used for oxidative reaction. The high-energy electrons from this oxidation are stored momentarily by reducing FAD to $FADH_2$. $FADH_2$ then reverts to FAD, sending its two high-energy electrons through the electron transport chain of Zn and Ca metal ions. The energy in $FADH_2$ is enough to catalyze the oxidation of glucose by the redox reaction.[49] $FADH_2$ can then be oxidized to the (semiquinone) FADH by donating one proton. The semiquinone is then oxidized once more by losing a proton and is returned to the initial quinone form (FAD). The oxidation of glucose is catalyzed by GOD and mediated by Zn and Ca ions. Binding of Zn and Ca ions to the GOD are redox-dependent. The glucose substrate bound by zinc loses electrons and is oxidized to gluconolactone and H_2O_2. The non-bridging oxygens in network structure of ZCSP-BNG lose electrons and then are utilized for the catalytic reaction (Figure 7d). In this way, Zn and Ca ions control the redox reaction of GOD. The substrate-enzyme and product-enzyme complexes are depicted in Figure 7e. The D-glucose substrate molecules first diffuse from the mesopores into the macropores and bind to the active sites of the GOD to form an enzyme-substrate complex. Then the substrate is converted into enzyme-product complex and attached to the GOD. Finally, the gluconolactone and H_2O_2 products are released from the mesopores, thus allowing the GOD to start all over again. This contributes to understanding how the metal-activated and binding GOD catalyzes glucose redox reactions.

3. Conclusions

The direct immobilization approach described above differs from single immobilization technique and has opened a new direction in integrating bioactive nanostructured glass with enzymatic catalytic reactions. The specially designed ZnO-CaO-SiO_2-P_2O_5 bioactive nanostructured glass has versatile hierarchical nanoporous structure, unique surface chemistry and potential for optimizing the catalytic reaction of enzymes.

Table 1. Codes of all the samples.

Yeast /ZnO or Fe_2O_3 or MgO	0 [mol%]	5 [mol%]	10 [mol%]	15 [mol%]
0 [wt%]	0ZCSP-BNG(0)	0ZCSP-BNG(5)	0ZCSP-BNG(10)	0ZCSP-BNG(15)
5 [wt%]	5ZCSP-BNG(0)	5ZCSP-BNG(5)	5ZCSP-BNG(10)	5ZCSP-BNG(15)
10 [wt%]	10ZCSP-BNG(0) 10FCSP (0) 10MCSP (0)	10ZCSP-BNG(5) 10FCSP (5) 10MCSP (5)	10ZCSP-BNG(10) 10FCSP (10) 10MCSP (10)	10ZCSP-BNG(15) 10FCSP (15) 10MCSP (15)
15 [wt%]	15ZCSP-BNG(0)	15ZCSP-BNG(5)	15ZCSP-BNG(10)	15ZCSP-BNG(15)

This new type of solid supporting material, namely, bioactive nanostructure phosphosilicate glass, gives both high affinity for enzyme molecules and a favored microenvironment that results in high immobilization efficiency with enhanced enzyme loading and stability compared to conventional approaches. Our approach is therefore economically advantageous and facile in operation. We expect that a rational design of bioactive nanostructure glass will lead to new immobilized approaches to entrap and stabilize different enzyme molecules for a wide range of applications such as a drug delivery vehicle, biosensor, nanobioreactor.

4. Experimental Section

Sample Synthesis: For a list of all chemicals, see the Supporting Information S4.1. As a typical synthesis procedure, yeast was used to prepare ZnO-CaO-SiO_2-P_2O_5 bioactive nanostructured glass (ZCSP-BNG) as the biotemplate. Generally, different amounts of yeasts and a certain amount of tetraethyl orthosilicate (TEOS), calcium nitrate tetrahydrate (CNT), zinc nitrate hexahydrate $Zn(NO_3)_3{\cdot}6H_2O$ (ZNH), triethyl phosphate (TEP) dissolved in ethanol and deionized water, respectively, giving a molar ratio of Si:(Ca+Zn or Fe or Mg): P = 50:46:5, and 0.85 mM $C_6H_8O_7{\cdot}H_2O$, then were mixed and stirred at room temperature for 6 h. The mixed solution was introduced into a sealed centrifuge tube and aged at 60 °C for 24 h, then dried at 60 °C for 48 h. The dried gel was calcined at 700 °C for 3 h to obtain the final products. The obtained ZnO-CaO-SiO_2-P_2O_5 bioactive nanostructured glass samples were denoted as xZCSP-BNG(y), where x and y represent the yeast/TEOS weight ratio and zinc oxide concentration, respectively. For instance, 5ZCSP-BNG(10) represents yeast/TEOS weight ratio and the content of zinc oxide were 5 wt% and 10 mol%, respectively. The others were the same means as 5ZCSP-BNG(10). The obtained Fe_2O_3-CaO-SiO_2-P_2O_5 and MgO-CaO-SiO_2-P_2O_5 glass samples were denoted as xFCSP(y) and xMCSP(y), respectively. The codes of all the samples are shown in **Table 1**. The characterization methods of samples see the Supporting Information S4.2. Biocompatibility tests in vitro see the Supporting Information S4.3.

Immobilization Experiments: For the immobilization of enzymes on the synthesized supports, 1 mL of the enzyme solution was added to 100 mg of synthesized support in a test tube at 4 °C for 12 h. The supernatant containing unreacted enzymes was separated from the supports by centrifugation for 5 min at 5000 rpm and 4 °C. The enzyme concentration of the supernatant was determined by a colorimetric method at 500 nm and was used for recalculation of the enzyme content of the supernatant. A mass balance for enzyme solution before and after immobilization was applied to calculate the amount of adsorbed enzyme using the Bradford method according to the Equation 10:[44]

$$A = \frac{Ci - Cs}{W} V \tag{10}$$

where A is the amount of enzyme bound onto ZCSP-BNG (mg g^{-1}, mg enzyme per gram support), Ci and Cs are the concentration of the enzyme initially added for immobilization and in the supernatant (mg mL^{-1}), respectively, V is the volume of the reaction medium (mL), and W is the weight of the support (g).

Enzymatic activity of free and immobilized GOD can be determined by measuring the initial rate of formation of hydrogen peroxide at a given temperature following the formation of a red quinoneimine dye, as mentioned by Rauf et al. (Figure 7a,b).[45] An assay mixture was prepared by pipetting 2 mL phenol-buffer, 0.5 mL β-D-glucose substrate, 0.5 mL horseradish peroxidase and 0.1 mL 4-aminoantipyrine (4-AAP) into a cuvette (d = 10 mm), respectively, and then incubated at 37 °C for 10 min. To start the enzymatic reaction, 0.1 mL of the supernatant solution was added to the cuvette and mixed well immediately. We keep the reaction mixture at 37 ± 0.1 °C and record the increase of absorbance at 500 nm in a spectrophotometer at specific intervals of 1 min (*A2* and *A5*, *A2*, *A5* refer to the absorbance of the reaction mixture exactly at 2 minutes and 5 min after the addition of enzyme solution) and calculate the ΔA per min using the linear portion of the curve (ΔAs). As a blank, pipette 0.1 M phosphate buffer into another cuvette (d = 10 mm) instead of GOD enzyme solution and take the same procedure described above (*Ab2* and *Ab5*). For comparison, control experiments were performed through the same assay procedure using the same amount of GOD without adding supports. GOD activity unit was denoted as U mL^{-1}, with one GOD activity unit (1 U) defined as the enzyme quantity which oxidizes 1 μmol of β-D-glucose per minute under the conditions described above.

The activity of the enzyme can be calculated using the following Equation (11):

$$\text{Activity (U mL}^{-1}) = \frac{(A_5 - A_2) - (A_{b5} - A_{b2})}{3} \times \frac{1}{12.88 \times 1/2} \times \frac{Dm}{0.1} \times 3.2 \tag{11}$$

where 3 is the reaction time (min), 12.88 denotes the millimolar extinction coefficient of quinoneimine dye, 1/2 is the factor based on the fact that two moles of H_2O_2 form one mole of quinoneimine dye, Dm is the dilution multiple of enzyme solution, 0.1 is the volume of enzyme solution, 3.2 is the final volume of the reaction mixture. Reusability experiments of immobilized enzyme see the Supporting Information S4.4. Optimum catalysis condition experiments of free and immobilized enzyme see Supporting Information S4.5.

Supporting Information

Supporting Information is available from the Wiley Online Library or from the author.

Acknowledgements

W.H., X.Z., and Y.Y. designed the experiments. D.M., Y.Z., and Z.B performed experiments and calculations. X.Z. and Y.Y. assisted in the initial stage of the project and experiments. W.H. wrote the paper. All authors discussed the results and commented on the manuscript. We thank Natural Science Foundation of China (Grant No. 51272144, 51172132, 51042003) and the Taishan Scholarship Program in the field of Glass and Ceramics for the technological support. We also

thank Natural Science Foundation of State Key Laboratory of Microbial Technology, Shandong University (Grant No. M2013–20) and National College Students' Innovative Entrepreneurial Training Plan Project (Grant No. 201310431029). We thank Caiyun Sun and Kewei Yang for helpful experiments.

Received: September 23, 2013
Revised: October 31, 2013
Published online: December 23, 2013

[1] S. J. Bao, C. M. Li, J. F. Zang, X. Q. Cui, Y. Qiao, J. Guo, *Adv. Funct. Mater.* **2008**, *18*, 591.
[2] Y. Li, Z. Y. Fu, B. L. Su, *Adv. Funct. Mater.* **2012**, *22*, 4634.
[3] F. Q. Tang, L. L. Li, D. Chen, *Adv. Mater.* **2012**, *24*, 1504.
[4] P. Y. Yang, S. L. Gai, J. Lin, *Chem. Soc. Rev.* **2012**, *41*, 3679.
[5] N. R. Haase, S. Shian, K. H. Sandhage, *Adv. Funct. Mater.* **2011**, *21*, 4243.
[6] S. S. Cao, L. Fang, Z. Y. Zhao, Y. Ge, S. Piletsky, A. P. F. Turner, *Adv. Funct. Mater.* **2013**, *23*, 2162.
[7] C. H. Lee, T. S. Lin, C. Y. Mou, *Nano Today* **2009**, *4*, 165.
[8] X. P. Wang, X. Li, K. Onuma, A. Ito, Y. Sogo, K. Kosuge, A. Oyane, *J. Mater. Chem.* **2010**, *20*, 6437.
[9] M. Zhu, L. X. Zhang, Q. J. He, J. J. Zhao, G. Limin, J. L. Shi, *J. Mater. Chem.* **2011**, *21*, 1064.
[10] G. Zoldak, A. Zubrik, A. Musatov, M. Stupak, E. Sedlak, *J. Biol. Chem.* **2004**, *279*, 47601.
[11] R. Esposito, B. D. Ventura, S. D. Nicola, C. Altucci, R. Velotta, D. G. Mita, M. Lepore, *Sensors* **2011**, *11*, 3483.
[12] S. Rauf, A. Ihsan, K. Akhtar, M. A. Ghauri, M. Rahman, M. A. Anwar, A. M. Khalid, *J. Biotechnol.* **2006**, *121*, 351.
[13] E. Tellechea, K. J. Wilson, E. Bravo, K. Hamad-Schifferli, *Langmuir* **2012**, *28*, 5190.
[14] Y. J. Song, K. J. Qu, C. Zhao, J. S. Ren, X. G. Qu, *Adv. Mater.* **2010**, *22*, 2206.
[15] D. E. Wilcox, *Chem. Rev.* **1996**, *96*, 2435.
[16] T. Kong, Y. Chen, Y. P. Ye, K. Zhang, Z. X. Wang, X. P. Wang, *Sens. Actuators, B.* **2009**, *138*, 344.
[17] Z. H. Dai, G. J. Shao, J. M. Hong, J. C. Bao, J. Shen, *Biosens. Bioelectron* **2009**, *24*, 1286.
[18] A. J. Salinas, S. Shruti, G. Malavasi, L. Menabue, M. Vallet-Regí, *Acta Biomater.* **2011**, *7*, 3452.
[19] S. Shruti, A. J. Salinas, G. Malavasi, G. Lusvardi, L. Menabue, C. Ferrara, P. Mustarelli, M. Vallet-Regì, *J. Mater. Chem.* **2012**, *22*, 13698.
[20] U. O. S. Seker, T. Ozel, H. V. Demir, *Nano Lett.* **2011**, *11*, 1530.
[21] Y. J. Lee, H. J. Yi, W. J. Kim, K. Kang, D. S. Yun, M. S. Strano, G. Ceder, A. M. Belcher, *Science* **2009**, *324*, 1051.
[22] X. G. Zhang, X. D. Zhang, W. He, Y. Z. Yue, H. Liu, J. Y. Ma, *Chem. Commun.* **2012**, *48*, 10093.
[23] X. G. Zhang, W. He, Y. Z. Yue, R. M. Wang, J. X. Shen, S. J. Liu, J. Y. Ma, M. Li, F. X. Xu, *J. Mater. Chem.* **2012**, *22*, 19948.
[24] X. Y. Du, W. He, X. D. Zhang, Y. Z. Yue, H. Liu, X. G. Zhang, D. D. Min, X. X. Ge, Y. Du, *J. Mater. Chem.* **2012**, *22*, 5960.
[25] M. Jensen, R. Keding, T. Hoche, Y. Z. Yue, *J. Am. Chem. Soc.* **2009**, *131*, 2717.
[26] C. J. Brinker, G. W. Scherer, *Sol-Gel Science: The Physics and Chemistry of Sol-Gel Processing*, Academic Press Inc., San Diego, USA **1990,** p.89.
[27] H. Gao, J. L. Yang, *Mod. Appl. Sci.* **2010**, *4*, 152.
[28] J. Chrusciel, L. Ślusarski, *Mater. Sci.* **2003**, *21*, 461.
[29] J. A. T. Barriga, D. G. Cooper, E. S. Idziak, D. R. Cameron, *Enzyme Microb. Tech.* **1999**, *25*, 96.
[30] Y. M. Wang, G. J. Du, H. Liu, D. Liu, S. B. Qin, N. Wang, C. G. Hu, X. T. Tao, J. Jiao, *Adv. Funct. Mater.* **2008**, *18*, 1131.
[31] B. Z. Tian, J. Liu, T. Dvir, L. H. Jin, J. H. Tsui, Q. Qing, Z. G. Suo, R. Langer, D. S. Kohane, C. M. Lieber, *Nat. Mater.* **2012**, *11*, 986.
[32] W. Vogel, Structure and Crystallization of Glasses, *Structure and Crystallization of Glasses*, Pergamon Press Ltd., Oxford, UK **1971**, p.59.
[33] M. K. Mahapatra, K. Lu, R. J. Bodnar, *Ap pl. Phys. A* **2009**, *95*, 493.
[34] J. E. Shelby, *Introduction to Glass Science and Technology*, 2nd Ed., The Royal Society of Chemistry, Cambridge, UK **2005**, p.127.
[35] R. R. Xu, W. Q. Pang, J. H. Yu, Q. S. Huo, J. S. Chen, *Science* **2004**, 124.
[36] T. Mosmann, *J. Immunol Methods* **1983**, *65*, 55.
[37] P. Sangsanoh, O. Suwantong, A. Neamnark, P. Cheepsunthorn, P. Pavasant, P. Supaphol, *Eur. Polym. J.* **2010**, *46*, 428.
[38] A. M. Chiorcea-Paquim, R. Pauliukaite, C. M. A. Brett, A. M. Oliveira-Brett, *Biosens. Bioelectron.* **2005**, *24*, 297.
[39] B. E. P. Swoboda, V. Massey, *J. Biol. Chem.* **1965**, *240*, 2209.
[40] L. Q. Cao, *Curr. Opin. Chem. Biol.* **2005**, *9*, 217.
[41] T. Xie, A. M. Wang, L. F. Huang, H. F. Li, Z. M. Chen, Q. Y. Wang, X, P. Yin, *AFR. J. Biotechnol.* **2009**, *8*, 4724.
[42] D. L. Morris, P. B. Ellis, R. J. Carrico, F. M. Yeager, H. R. Schroeder, J. P. Albarella, R. C. Bogustaski, W. E. Hornby, D. Rawson, *Anal. Chem.* **1981**, *53*, 658.
[43] C. M. Harris, A. M. Derdowski, C. D. Poulter, *Biochim.* **2002**, *41*, 10554.
[44] C. G. Lei, Y. S. Shin, J. Liu, E. J. Ackerman, *Nano Lett.* **2007**, *7*, 1050.
[45] P. J. Li, F. P. Zhang, *J. Non-Cryst. Solids* **1990**, *119*, 112.
[46] L. T. Zhuravlev, *Langmuir* **1987**, *3*, 316.
[47] C. J. Brinker, G. W. Scherer, *Sol–Gel Science: The Physics and Chemistry of Sol–Gel Processing*, Academic Press Inc., San Diego, USA, **1990**, pp.14 and 184.
[48] S. Rauf, A. Ihsan, K. Akhtar, M. A. Ghauri, M. Rahman, M. A. Anwar, A. M. Khalid, *J. Biotechnol.* **2006**, *121*, 351.
[49] D. Astruc, *Nature Chem.* **2012**, *4*, 255.